**Cell Reports, Volume *24***

## Supplemental Information

# Phosphatidylserine Externalization Results from and Causes Neurite Degeneration in *Drosophila*

**Maria L. Sapar, Hui Ji, Bei Wang, Amy R. Poe, Kush Dubey, Xingjie Ren, Jian-Quan Ni, and Chun Han**

**SUPPLEMENTAL INFORMATION**

**SUPPLEMENTAL FIGURES**

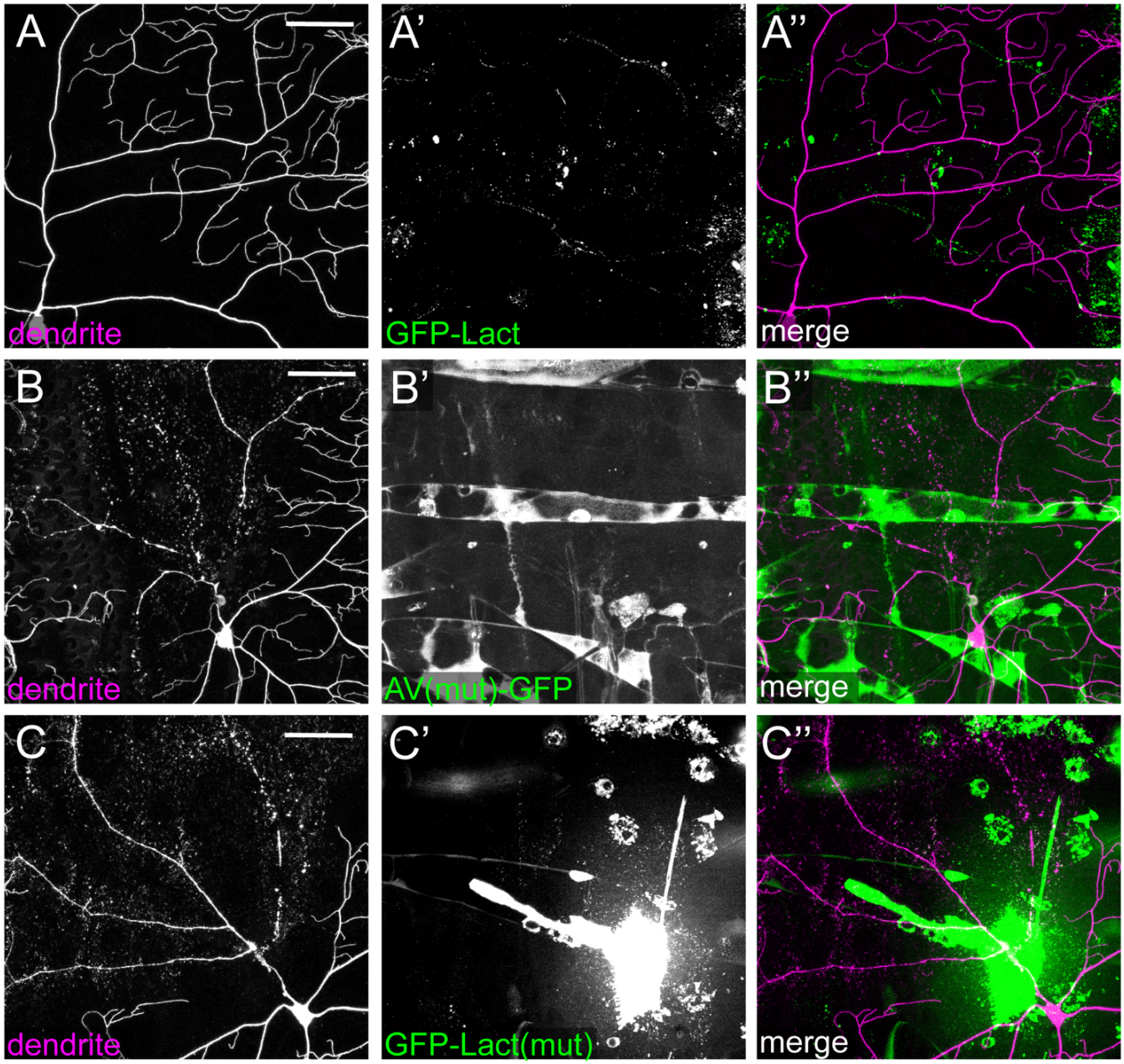


**Figure S1. Mutant PS sensors do not bind to degenerating dendrites, related to Figure 1.**

(A-A") An uninjured C4da neuron in the presence of Lact-GFP.

(B-B") Injured C4da dendrites in the presence of AV (mut)-GFP at 4-5 hours AI

(C-C") Injured C4da dendrites in the presence of GFP-Lact (mut) at 4-5 hours AI.

Scale bars represent 50 μm.

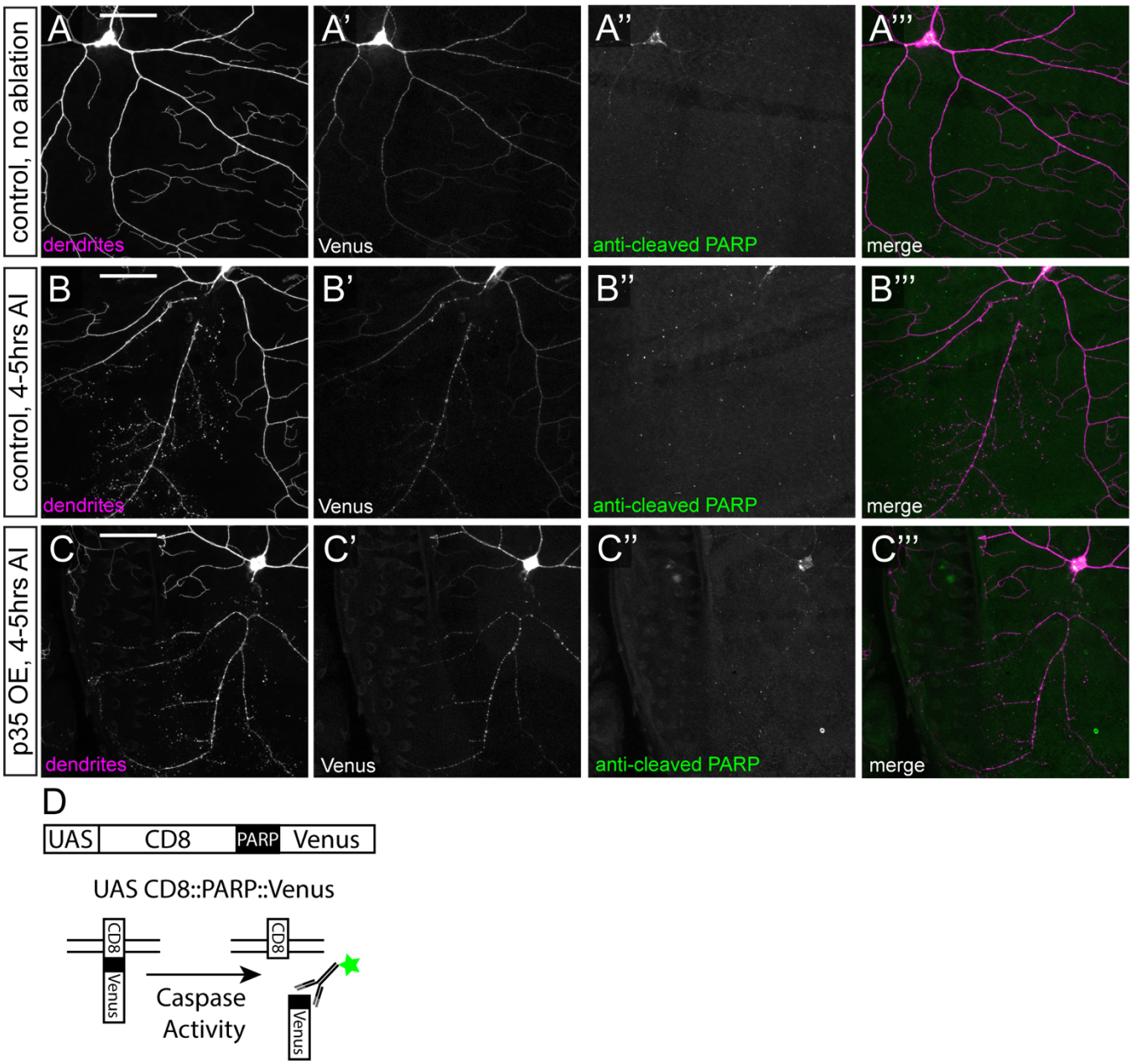


**Figure S2. Injury of C4da neurons does not lead to caspase activity at 4 hrs AI, related to Figure 2.**

(A-B''') Anti-cleaved PARP staining in uninjured (A-A''') and injured (B-B''') wildtype neurons.

(C-C''') Anti-cleaved PARP staining in injured p35 expressing (C-C''') dendrites.

(D) Schematic representation of CD8::PARP::Venus, the cleavage of which by caspases exposes a unique epitope that can be recognized by a specific antibody (adapted from Williams et al., 2006). The antibody appears to show some weak background binding to noncleaved PARP. Injured dendrites of neither wildtype neurons nor p35-expressing neurons showed higher than background staining.

Scale bars represent 50 μm.

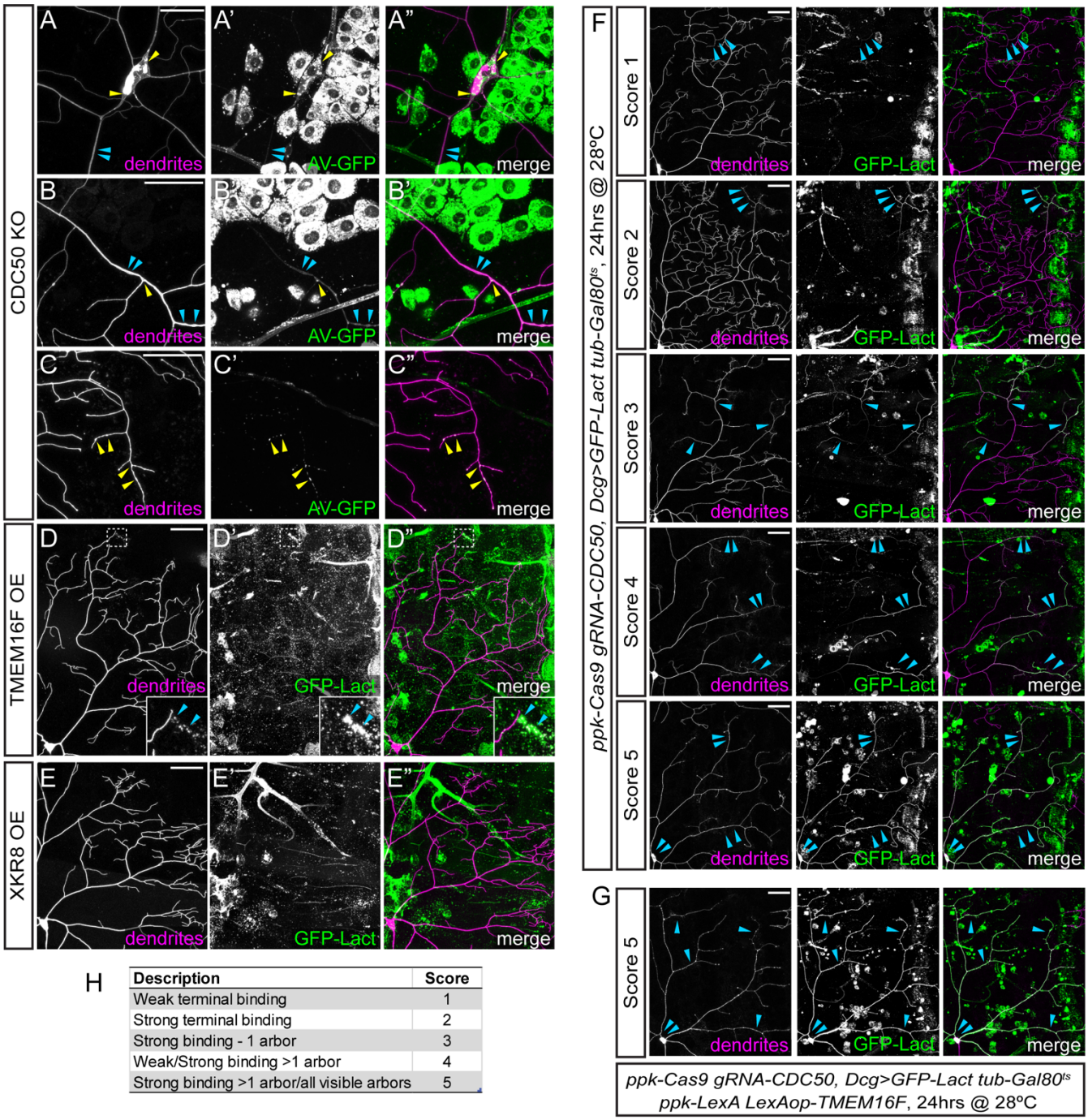


H

| Description | Score |
|---|---|
| Weak terminal binding | 1 |
| Strong terminal binding | 2 |
| Strong binding - 1 arbor | 3 |
| Weak/Strong binding >1 arbor | 4 |
| Strong binding >1 arbor/all visible arbors | 5 |

**Figure S3. PS exposure on *CDC50* knockout and scramblase overexpression neurons, related to Figure 3.**

(A-C) Labeling of *CDC50* KO neurons by AV-GFP, showing a cell body and primary branches (A-A"), primary branches (B-B"), distal dendrites (C-C"). Blue arrowheads point to smooth labeling and yellow arrowheads point to intracellular puncta.

(D-D") Dendrites of a TMEM16F OE neuron labeled by constitutively expressed GFP-Lact. Inset shows dendrite debris labeled by GFP-Lact.

(E) Dendrites of an XKR8 OE neuron in the presence of constitutively expressed GFP-Lact. No obvious dendrite labeling was detected.

(F) Scoring system for quantifying the binding of transiently expressed GFP-Lact on *CDC50* KO neurons and *CDC50* KO +

TMEM16F OE neurons. Representative *CDC50* KO neurons are shown. Blue arrowheads indicate GFP-Lact binding.

(G) Example of a *CDC50* KO + TMEM16F OE neuron that received a score of 5

(H) Description of GFP-Lact labeling and corresponding scores.

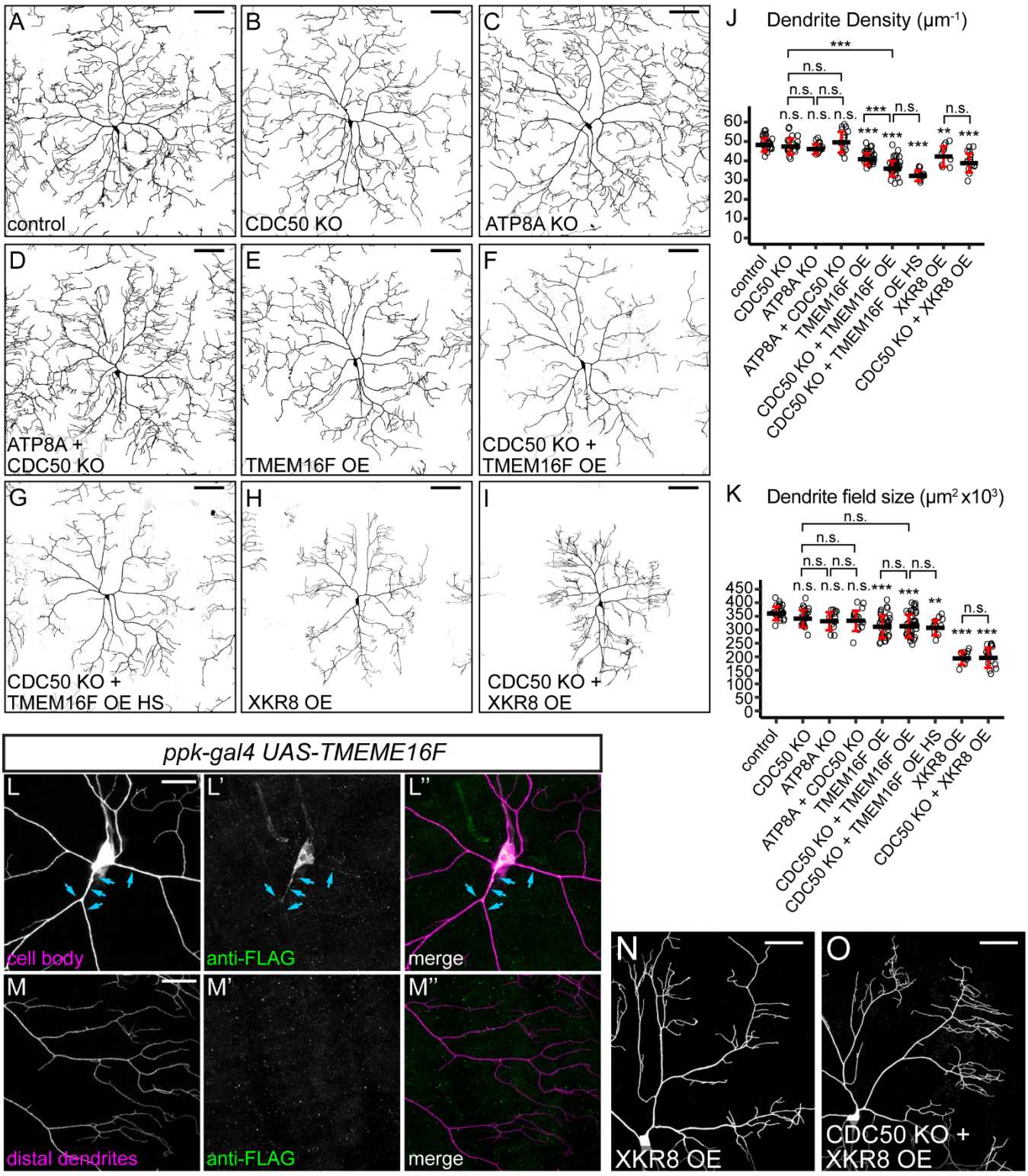


**Figure S4. Dendrite morphologies of flippase knockout neurons and scramblase overexpressing neurons, related to Figure 4.**

(A-I) Dendritic fields of control (A), *CDC50* KO (B), *ATP8A* KO (C), *CDC50* and *ATP8A* double KO (D), TMEM16F OE (E), *CDC50* KO + TMEM16F OE (F), heat-shocked *CDC50* KO + TMEM16F OE (G), XKR8 OE (H), and *CDC50* KO + XKR8 OE (I) neurons.

(J and K) Quantification of dendrite density (J) and dendrite field size (K) in indicated genotypes. n = number of neurons: control (n=24, 11 animals); *CDC50* KO (n=21, 11 animals); *ATP8A* KO (n=13, 9 animals); *ATP8A* + *CDC50* KO (n=16, 9 animals); TMEM16F OE (n=34, 19 animals); *CDC50* KO + TMEM16F OE (n=41, 26 animals); *CDC50* KO + TMEM16F OE HS (n=11, 7 animals); XKR8 OE (n=10, 8 animals); *CDC50* KO + XKR8 OE (n=16, 9 animals). **p≤0.01, ***p≤0.001, n.s., not significant; One-way ANOVA and Tukey's HSD test. Black bar, mean; red bars, SD.

(L-M") Anti-Flag staining of TMEM16F in the cell body and primary branches (L-L") and distal dendrites (M-M"). Blue arrows indicate anti-Flag signals.

(N-O) Partial dendritic fields of XKR8 OE (N) and *CDC50* KO + XKR8 OE (O) C4da neurons showing the level of dendritic debris in epidermal cells.

Scale bars represent 100 μm in (A-I) and 25 μm in (M) and (L) and 50 μm in (N) and (O)

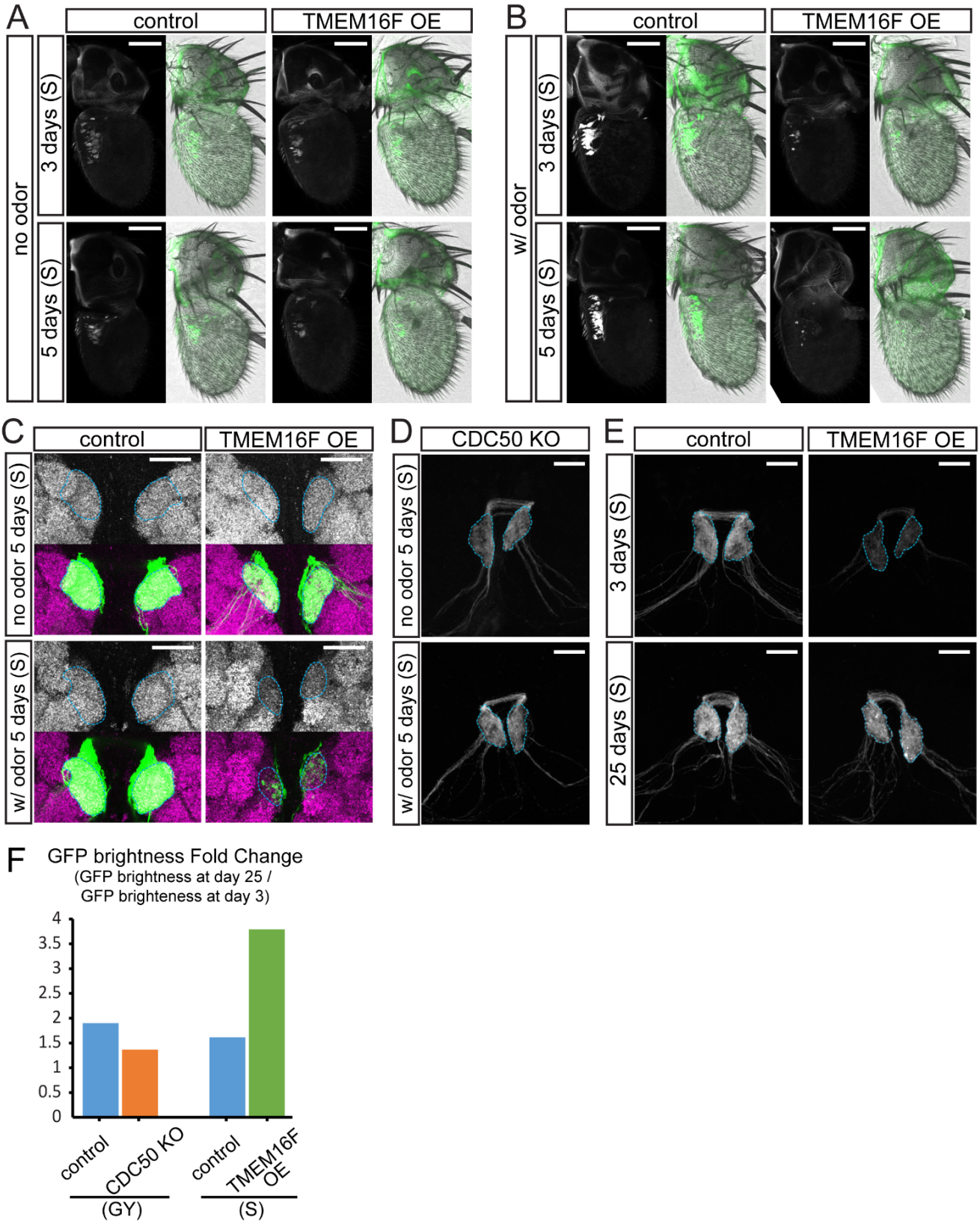


**Figure S5. Flippase loss and scramblase overexpression cause distinct modes of axonal degeneration in the adult fly brain, related to Figure 6.**

(A and B) Antennae of control and TMEM16F-overexpressing flies that were not exposed to odors (A) or exposed to ethyl butyrate (B) to show GFP signals at the cell bodies of Or22a ORNs.

(C) DM2 glomeruli of control and TMEM16F-overexpressing 5-day-old flies that were exposed or not exposed to ethyl butyrate. Anti-Brp (nc82) staining is in grey in each upper panel or in magenta in each merged panel. DM2 glomeruli are outlined.

(D) Axons of CDC50 KO Or22a ORNs in 5-day-old adult flies that were exposed or not exposed to ethyl butyrate.

(E) Axons of control and TMEM16F-overexpressing Or22a ORNs in 3-day-old and 25-day-old adult brains in the absence of odor exposure.

(F) Fold change of GFP levels between 3 and 25 days in genotypes shown.

The type of fly media used for each experiment is indicated: S – sucrose agar; GY – glucose yeast food. In all image panels, Or22a glomeruli are outlined. Scale bars represent 50 μm in (A and B) and 20 μm in (C-E).

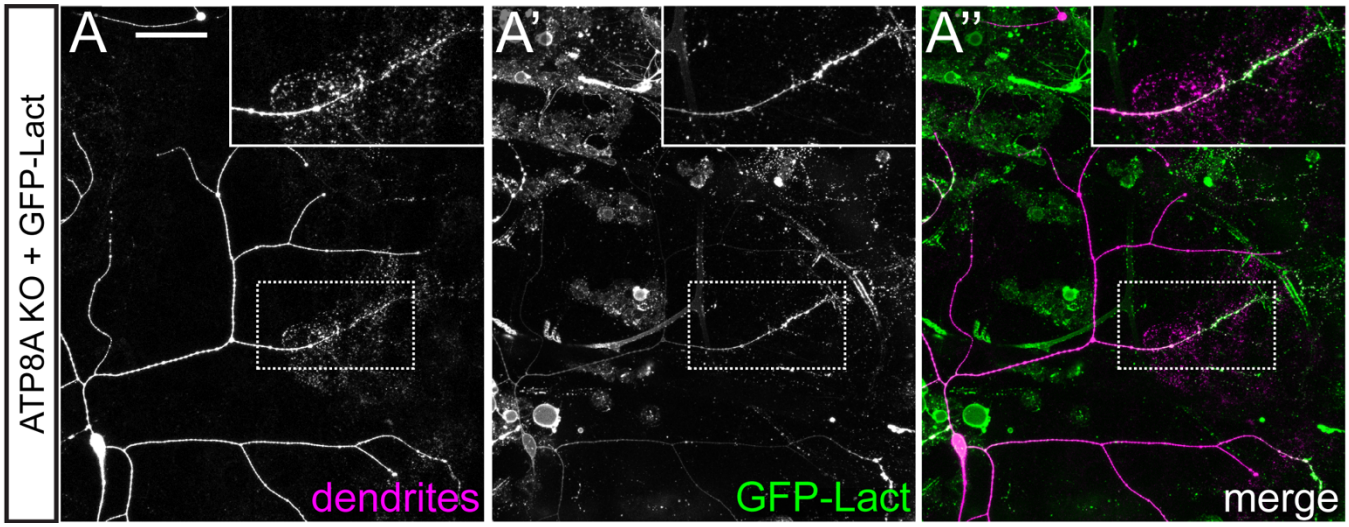


**Figure S6. Constitutively expressed GFP-Lact causes *ATP8A* knockout neurons to degenerate, related to Figure 7.**

(A-A") Dendrites of an *ATP8A* KO neuron in the presence of constitutively expressed GFP-Lact. Inset shows a degenerating dendrite with high GFP-Lact labeling. The scale bar represents 50 μm.

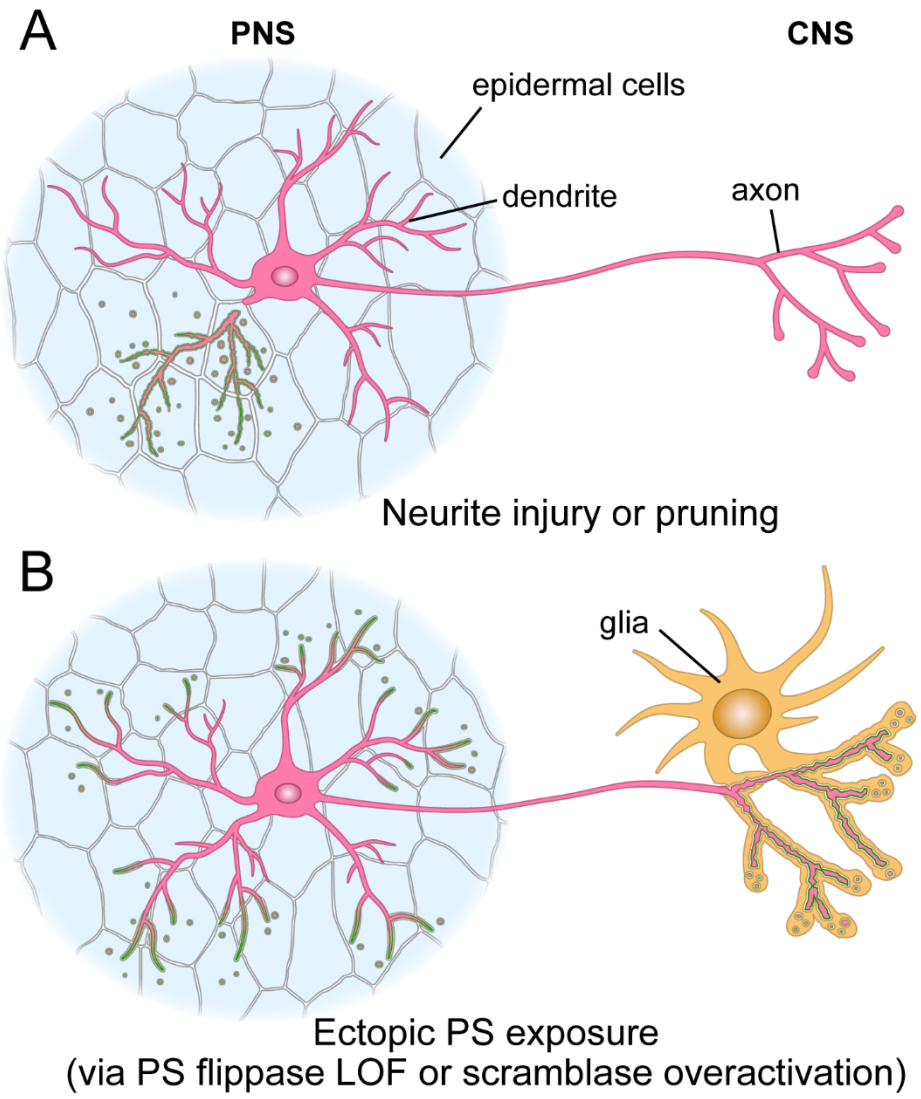


**Figure S7. PS exposure is a result and a cause of neurite degeneration, related to Figure 6.**

(A) During neurite injury or pruning, detached neurites expose PS (green) as an event of the degeneration program. Resident phagocytes such as epidermal cells recognize PS-exposing neurites and engulf neurite debris.

(B) Loss of PS flippases or overactivation of scramblases result in PS exposure on distal neurites, which causes resident phagocytes, such as epidermal cells in the PNS and glia in the CNS, to attack and break down PS-exposing neurites. The involvement of glia in this model is inferred from previous studies (MacDonald et al., 2006; Freeman, 2015).

## SUPPLEMENTAL EXPERIMENTAL PROCEDURES

### Fly strains

*ppk-CD4-tdTom* (Han et al., 2011), *ppk-MApHS* (Han et al., 2014), *ppk-Gal4* (Han et al., 2012), *UAS-CD4-tdTom* (Han et al., 2011), *tubP-Gal80$^{ts}$* (McGuire et al., 2003), *ppk-LexA* (Poe et al., 2017), *Dcg-Gal4* (Suh et al., 2006), *UAS-Wld$^{s}$* (MacDonald et al., 2006), *Or22a-Gal4* (Dobritsa et al., 2003), and *UAS-mCD8-GFP* (Lee and Luo, 1999) have been previously described. *UAS-p35* (BDSC 5072) and *UAS-Diap1* (BDSC 6657) were obtained from Bloomington Stock Center (BDSC).

### Molecular cloning and transgenic flies

UAS-driven PS sensors were constructed in pIHEU-MCS (Addgene 58375), an insulated high-expression UAS vector that is compatible with both φC31-mediated integration and P-element-mediated transformation. pIHEU contains 5xUAS, a HIH cassette (*hsp70* core promoter-5′UTR, a chimeric intron, and *His2Av* 3′UTR-polyA) that supports high transgene expression in *Drosophila* (Han et al., 2011), and two copies of gypsy insulators that reduce positional effect-related leaky expression. To construct pIHEU-MCS, an SphI-XbaI fragment was isolated from pACU2 (Han et al., 2011) and cloned into SphI/XbaI sites of pAPIC-CD4-tdGFP (Han et al., 2011).

*UAS-AV-GFP* and *UAS-AV(mut)-GFP*: From 5' to 3', a Syn21-Akh SP fragment, human Annexin V (AV) coding sequence, and superfolder GFP (sfGFP) coding sequence were cloned into pIHEU-MCS between EcoRI/XbaI sites. Syn21 (aacttaaaaaaaaaaatcaaa) (Pfeiffer et al., 2012) is a translation enhancer sequence before the start codon. Akh SP (Han et al., 2011) encodes a signal peptide for AV-GFP secretion. AV and AV(mut) fragments were PCR-amplified from pJM31AnxV::GFP and pJM62 AnxVMut::GFP (Mapes et al., 2012) (gifts from Ding Xue, University of Colorado Boulder), respectively, using primers aaaagctagcGCACAGGTTCTCAGAGGC and aaaaaagcttGTCATCTTCTCCACAGAGCAG and subsequently digested by NheI and HindIII. sfGFP was PCR-amplified from pBS-sfGFP (a gift from Thomas Kornberg, University of California, San Francisco) using primers aaaaaagcttggtggcggcggaagtggaggtggaggctcgATGTCCAAGGGCGAGGAG and aatttctagaTTACTTGTACAGCTCATCCATGCCCAG and subsequently digested by HindIII and XbaI.

*UAS-GFP-Lact* and *UAS-GFP-Lact(mut)*: From 5' to 3', the Syn21-Akh SP fragment, sfGFP coding sequence, and mouse lactadherin (Lact) C1C2 coding sequence were cloned into pIHEU-MCS between EcoRI/XbaI sites. sfGFP was PCR-amplified from pBS-sfGFP using primers ataagctagcagtATGTCCAAGGGCGAGGAG and aaaaaagcttcgagccaccaccgccacttccgccgccaccggaCTTGTACAGCTCATCCATGCCCAG and subsequently digested by NheI and HindIII. LactC1C2 and LactC1C2(mut) were PCR-amplified from pJM483 GFP::LactC1C2 and pJM656 GFP::LactC1C2(Mut) (Mapes et al., 2012) (gifts from Ding Xue, University Colorado Boulder), respectively, using primers aaaaaagcttCGCTGTTCTACACAGCTGGGCATGGAAGGGGG and aatttctagaTTAACAGCCCAGCAGCTCCAG and subsequently digested by HindIII and XbaI.

*UAS-AV-mCard*: Syn21-Akh SP-AV and mCardinal (mCard) coding sequence (Chu et al., 2014) were cloned into EcoRI/XbaI sites of pIHEU-MCS. The Syn21-Akh SP-AV fragment was isolated from pIHEU-AV-sfGFP by EcoRI/HindIII digestion. The mCard fragment was PCR-amplified from pcDNA3-mCardinal (Addgene 51311) using primers aaaaaagcttggtggcggcggaagtggaggtggaggctcgATGGTGAGCAAGGGCGAGG and aatttctagaTTACTTGTACAGCTCGTCCATGCC and subsequently digested by HindIII/XbaI.

*LexAop-GFP-Lact*: An Syn21-Akh SP-AV-sfGFP fragment was isolated from pIHEU-AV-sfGFP by EcoRI/XbaI digestion and then cloned into EcoRI/XbaI sites of pAPLO (Poe et al., 2017).

*LexAop-AV-mCard*: The Syn21-Akh SP-AV-mCard fragment was isolated from pIHEU-AV-mCard by EcoRI/XbaI digestion and cloned into EcoRI/XbaI sites of pAPLO.

UAS-XKR8 and UAS-TMEM16F were constructed in pACUH (Addgene 58374), a UAS vector that is compatible with both φC31-mediated integration and P-element-mediated transformation. pACUH contains 10xUAS, *hsp70* core promoter-5′UTR, and *SV40* 3′UTR-polyA, and drives weaker transgene expression than pIHEU-MCS. To construct pACUH, a fragment containing the attB sequence was first inserted into the NdeI site of pUAST (Brand and Perrimon, 1993) to make pACU. The 5xUAS in pACU was then replaced with a 10xUAS fragment.

*UAS-XKR8*: XKR8-Flag coding sequence was PCR-amplified from pMXs-puro mXkr8-GFP (a gift from Shigekazu Nagata, Osaka University) using primers aaaaGAATTCaaaATGCAGATGATGACTAGGAAGGTCC and aattTCTAGAttacttgtcgtcgtcgtccttgtagtcgccGAGGACTCCATTCAGCTGCACCTCCTCTGTC, and subsequently cloned into EcoRI/XbaI sites of pACUH.

*UAS-TMEM16F*: TMEM16F-D430G-L-Flag coding sequence was PCR-amplified from pMXs-puro mTMEM16F D430G-L FLAG (a gift from Shigekazu Nagata, Osaka University) using primers aaaaGAATTCaaaATGCAGATGATGACTAGGAAGGTCC and aaaaGAATTCaaaATGCAGATGATGACTAGGAAGGTCC, and subsequently cloned into EcoRI/XbaI sites of pACUH.

*LexAop-Xkr8* and *LexAop-TMEM16F*: XKR8-Flag and TMEM16F D430G-L-Flag were isolated from pACUH-Xkr8-Flag and pACUH-TMEM16D430G-Flag, respectively, by EcoRI/XbaI digestion and cloned into EcoRI/XbaI sites of pAPLO3. pAPLO3 is similar to pAPLO but only has 11x LexAop2 and no intron. pAPLO3 is expected to drive lower transgene expression than pAPLO.

*R16A03-lexA*: The R16A03 enhancer was PCR amplified from R16A03-Gal4 (BDSC 45809) genomic DNA using primers ggggACAAGTTTGTACAAAAAAGCAGGCTGGGGAGAGTTGCCGTATCATTTTGGCTTATTGG and ggggACCACTTTGTACAAGAAAGCTGGGTGTCTCGACTAGCTTCCTGCTCAACCTGC. The resultant DNA fragment was used to create an entry vector through a Gateway BP reaction (Thermo Fisher Scientific). The entry vector was then combined with pBPLexA::p65Uw (Addgene 26231) to generate pR16A03-LexAp65 expression vector through a Gateway LR reaction.

The above constructs were injected in house or by Rainbow Transgenic Flies to transform flies through φC31 integrase-mediated integration into attP docker sites.

**Generation of *drpr$^{indel}$* allele by CRISPR/Cas9**

A gRNA-drpr expression vector was constructed using the U6b-sgRNA-short vector (Ren et al., 2013) and the targeting sequence GGTAATCCTCATAGCCTGCC. gRNA-drpr plasmid DNA was then injected into *nos-Cas9$^{attP2}$* embryos. The resulting flies were crossed with TM6B balancer flies to isolate individual progeny carrying mutations at the targeting sequence. Indel mutations were detected by the loss of a BglI site in genomic PCR products amplified by primers ACGTCATAAACTCATCCGACGGG and CCAACTCACCACAACAGTCCCTC. Sequencing of *drpr$^{indel}$* homozygous flies confirmed that 2 nucleotides (CT) were inserted after the T in the 9$^{th}$ codon, causing a reading frame shift mutation. Because the next in-frame methionine codon (AA143) is after the signal peptide (AA1-AA30), alternatively translated proteins should not be properly processed and targeted to the plasma membrane. Therefore, *drpr$^{indel}$* is predicted to behave as a null allele.

**Tissue-specific gene knockout via CRISPR/Cas9**

Tissue-specific gene knockout in C4da neurons was achieved by crossing flies carrying *ppk-Cas9* and flies ubiquitously expressing two gRNAs targeting the gene of interest. *ppk-Cas9* is similar to *ppk-CD4-tdTom* except that the coding sequence is from *S. pyogenes* Cas9 gene. The transgenic gRNA constructs were similar to pCFD4-U6.1_U6.3 except that the selection marker is mini-white (Port et al., 2014). The details of the construction and characterization of *ppk-Cas9* and gRNA vectors will be published elsewhere. For tissue-specific gene knockout in adult Or22a ORNs, *Or22a-Gal4* was used to drive *UAS-Cas9* expression so that CRISPR/Cas9-mediated knockout only occurred in mature neurons.

We used two gRNA predictor tools, sgRNA Scorer 2.0 (https://crispr.med.harvard.edu) and Benchling (www.benchling.com), to identify candidate gRNA targeting sequences with high on-target scores in both algorithms. For each gene, we selected two targeting sequences that are against coding exons of all splicing isoforms and are predicted not to have alternative target sites by both algorithms. The targeting sequences are GGTGTGGTATACATGTACTACGG and GTCAAGTTCCGAAACCCAGAGGG for *CDC50* and ATCATCTGCATCGTACCCAGCGG and AAGTTCGCGAGCAACTTCCGCGG for *ATP8A* (the PAM sequences are underlined and not included in the final gRNA vectors). The constructs were injected by Rainbow Transgenic Flies to transform attP docker lines using φC31 integrase-mediated transformation, with *gRNA-CDC50* inserted to *attP$^{2}$* and *gRNA-ATP8A* inserted to *attP$^{VK19}$*.

**Testing gRNA efficiency**

To test gRNA efficiency, homozygous males of gRNA for target gene were crossed to *Act-Cas9 lig4* homozygous females. The embryo density was controlled (around 100 embryos per vial) and the vials were monitored every day to record the animal lethal phase. As *Act-Cas9* and the *lig4* null mutation are both on the X chromosome, the male progeny from the cross is *lig4* deficient and therefore cannot repair DNA double-stranded breaks (DSBs) through NHEJ. In contrast, the female progeny is heterozygous for *lig4* and thus can repair DSBs. Efficient gRNAs will target the gene locus to create bi-allelic DSBs, which will be repaired to generate indels in female somatic cells but left unrepaired in male somatic cells. If target gene is a non-essential gene, female progeny with indel mutations at the gene locus should be viable while male progeny will die in the pupal stage due to the lack of the DSB repair. If target gene is an essential gene, target gene LOF will cause both female and male progeny to die to at a stage similar to the lethal phase of target gene zygotic null mutants. Viable male progeny from this cross indicates inefficient gRNAs. It is also possible, if the gRNA is inefficient but the gene is essential, female progeny may survive. The *gRNA-CDC50* efficiency test resulted in lethality at 1$^{st}$ to 2$^{nd}$ instar larval stages for most animals and rarely at 3$^{rd}$ instar, suggesting that the gRNA line is efficient. For *gRNA-ATP8*, only adult females emerged. It possible that ATP8 is a nonessential gene and the gRNA line is very efficient, or that *ATP8A* is an essential gene but the gRNA line is only moderately efficient.

**Live imaging**

Animals were reared at 25°C in density-controlled vials (60-100 embryos/vial) on standard yeast-glucose medium (doi:10.1101/pdb.rec10907). Larvae at 125 hours AEL (wandering stage) were mounted in 100% glycerol under coverslips with vacuum grease spacer and imaged using a Leica SP8 microscope equipped with a 20X NA0.75 multi-immersion

objective for quantifying dendritic field sizes and length and a 40X NA1.30 oil objective for others. For imaging with the 40X objective, larvae were lightly anesthetized with isoflurane before mounting. For consistency, we imaged dorsal ddaC neurons from A1-A3 segments (2-3 neurons per animal) on one side of the larvae. For imaging GFP-Lact labeling of *CDC50* KO and *CDC50* KO + TMEM16F OE neurons, we imaged ddaC neurons on both sides of the larvae and hence 3-5 neurons per animal. Unless stated otherwise, confocal images shown in all figures are maximum intensity projections of z stacks encompassing the epidermal layer and the sensory neurons beneath, which are typically 8–10 μm for larvae and 12–15 μm for pupae.

*Injury assay*

For dendrite lesion, larvae at 90 hr AEL were lightly anesthetized with isoflurane, mounted in a small amount of halocarbon oil (Halocarbon Products Corporationt) under coverslips with grease spacers. The laser ablation was performed on a Zeiss LSM880 Confocal/Multiphoton Upright Microscope, using a 790 nm two-photon laser at primary dendrites of ddaC neurons in A1 and A3 segments. The laser power was set at 80% and number of laser pulses/iterations = 20. Animals were recovered on grape juice agar plates following lesion for appropriate time (4-5 hr or 9-10 hr). After recovery, the larvae were either mounted in 100% glycerol under coverslips with grease spacers and imaged using a Leica SP8 microscope or imaged with the long-term time-lapse imaging method.

*Long-term time-lapse imaging*

Long-term time-lapse imaging at the larval stage was done as described previously (Poe et al., 2017) with small modifications. Briefly, a layer of double-sided tape was placed on the coverslip to define the position of PDMS blocks. A small amount of UV glue was added to the groove of PDMS and to the coverslip. Anesthetized larvae were placed on top of the UV glue on the coverslip and then covered by PDMS blocks with the groove side contacting the larva. Glue was then cured by 365nm UV light. The coverslip with attached PDMS and larvae was mounted on an aluminum slide chamber that contained a piece of moisturized Kimwipes (Kimtech Science) paper. Time-lapse imaging was performed on a Leica SP8 confocal with a 40x NA1.3 oil objective at digital zoom 0.75 and a 3-min interval. For ablation experiments, larvae were recovered after injury on grape agar plates for 1.5-2 hours before mounting and imaging. For long-term time-lapse imaging of dendrite pruning, white pupae were directly mounted in the imaging chamber similar to larval mounting and kept on the imaging chamber for 4-6 hours before imaging.

*Antenna imaging*

Flies were washed in ethanol, the antennae were removed, allowed to briefly dry and then were mounted in 100% glycerol on charged Diamond White Glass microscope slides (Globe Scientific, 1358W) with vacuum grease (Dow Corning) as spacers between coverslips and slides. The antennae were imaged under Leica SP8 microscope with a 40x NA1.3 oil objective.

*Transient expression of GFP-Lact*

Animals expressing *dcg-Gal4 UAS-GFP-Lact* and *tubP-Gal80ts* were kept at 18°C until late 3$^{rd}$ instar. The vials were then transferred to and kept in 28°C incubator for 24 hours. Wandering larvae were then selected from the vials for imaging. For injury after induction of GFP-Lact, animals were laser injured after 32-hour incubation at 28°C and then were recovered on grape agar plates for 3-4 hours at 28°C before imaging.

*Larval heat shock treatment*

Larvae at 125 hours AEL were placed in a chamber made of two opposing 35 mm petri dishes which was sealed with Parafilm (Bemis NA). The chamber was then subject to three 2-min heat shocks in 42°C water bath with 10-min intervals. Larvae were then recovered on moisturized petri dishes for 30 min at 25°C before imaging.

*Labeling of PS exposure*

To visualize in vivo PS exposure in larvae or pupae, we used the following combinations of drivers and PS sensors for each experiment. For injury and pruning: *Dcg-Gal4 UAS-AV-GFP* or *Dcg-Gal4 UAS-GFP-Lact*; for overexpression of Wld$^{s}$, p35, or Diap1: *R16A03-LexA LexAop-GFP-Lact* with *ppk-Gal4 UAS-Wld$^{s}$*, *UAS-p35*, *or UAS-Diap1*; for examining PS exposure due to *CDC50*/*ATP8* KO: *Dcg-Gal4 UAS-AV-GFP* or *Dcg-Gal4 UAS-GFP-Lact* with *ppk-Cas9 gRNA*; for PS exposure due to TMEM16F/XKR8 OE: *R16A03-LexA LexAop-AV-mCard* or *LexAop-GFP-Lact* with *ppk-Gal4 UAS-TMEM16F*, *or UAS-XKR8*; for *CDC50* KO + TMEM16 OE: *Dcg-Gal4 UAS-GFP-Lact*, ppk-LexA LexAop-TMEM16F, and *ppk-Cas9 gRNA-CDC50*.

Some experiments involving multiple genetic components, which required the use of recombinant flies containing both the driver and the PS sensor in genetic crosses. Because recombination of Annexin V with either Gal4 or LexA driver yielded animals with low fecundity, we used GFP-Lact only for those experiments.

**Adult brain experiments**

For experiments examining Or22a axon degeneration in *CDC50* KO animals, newly emerged adults were kept at 25°C for 3 days or 25 days on glucose-yeast medium prior to dissection. For experiments examining Or22a axon degeneration in TMEM16F OE animals, newly emerged adults were kept at 25°C for 3 days or 25 days on sucrose (8%) agar medium prior to dissection. For odor test, 20µl of 1% (v/v) ethyl butyrate dissolved in mineral oil was dotted on a small piece of filter paper, which was then placed on the top of sucrose (8%) agar medium in fly vials. As a control, 20 µl of mineral oil was dotted on filter paper. Newly emerged adults were separated into two groups: experimental groups were kept in vials with ethyl butyrate filter paper; control groups were kept in vials with mineral oil paper. All animals were transferred to fresh vials every day for 5 days prior to dissection. For all brain experiments, we did not detect difference between male and female brains but we only showed results from male brains for consistency.

Brain dissection was performed in PBST (0.2% Triton-X in PBS). Dissected brains were fixed in 4% formaldehyde in PBS for 20 min and then rinsed with PBST three times. Same staining protocol was used for brains as for larval body walls. Brains were mounted in SlowFade® Diamond Antifade Mountant (Thermo Fisher Scientific) on charged Diamond White Glass microscope slides (Globe Scientific, 1358W) with vacuum grease (Dow Corning) as spacers between coverslips and slides. The brains were imaged under Leica SP8 microscope with a 40x NA1.3 oil objective.

**Immunohistochemistry**

The antibodies used in this study are mouse monoclonal Anti-FLAG M2 antibody (Sigma F3165, 1:250), rabbit anti-cleaved PARP1 antibody(Abcam ab2317, 1:500), mouse anti-Brp (NC82) (Developmental Studies Hybridoma Bank , 1:100), rabbit anti-GFP secondary antibody conjugated to Alexa Fluor 488 (Life Technologies A-21311, 1:500), and donkey secondary antibody conjugated to Alexa Fluor 488 (Jackson ImmunoResearch 715-545-150, 1:400) or Alexa Fluor 647 (Jackson ImmunoResearch 711-605-152, 1:400). Immunostaining of *Drosophila* larval body walls was performed as previously described (Poe et al., 2017). Briefly, 3rd instar larvae were dissected in cold PBS, fixed in 4% formaldehyde/PBS for 30 min at room temperature, and stained with the primary antibody overnight at 4°C and subsequently the secondary antibody for 2 hours at room temperature. Fillets were then mounted for microscopy. For brain staining, same immunohistochemistry protocol was followed as for larva body wall staining. The brains were imaged under Leica SP8 microscope with a 40x NA1.3 oil objective.

**Image analysis and quantification**

Image processing and analyses were done in Fiji/ImageJ. Methods for tracing and measuring C4da neuron dendrites have been previously described (Poe et al., 2017). For dendrite debris measurement, each Z-projected image (1,024 x 1,024 pixels) taken with a 40X objective was first processed to generate a dendrite mask through Gaussian Blur (Sigma: 1), Auto Local Threshold (Phansalkar method, radius: 50), Particles8 plugin (to remove particles smaller than 200 pixels), and Dilate (iterations=2, count=1). The signals within the dendrite mask were removed and the debris outside the dendrite mask was converted to a debris mask by thresholding with fixed thresholds (40, 255). The region of interest (ROI) for measurement was defined as the area within one-epidermal-cell diameter (40 µm) from dendrites in the dorsal posterior quadrant of the ddaC dendritic field. We only considered the region within one-epidermal-cell diameter (40 µm) from dendrites in order to correct for situations in which dendrites are very sparse. The dendrite pixel area ($A_{den}$) and debris pixel area ($A_{deb}$) in the ROI were measured and dendrite coverage ratio was calculated based on the following formula: $A_{deb} \cdot A_{ROI} / (A_{ROI} - A_{den}) \cdot A_{den}$. To measure debris level in relation to the distance from the cell body, we used the Sholl Analysis plugin (https://imagej.net/Sholl_Analysis) on dendrite and debris masks. Debris particle numbers and (terminal) dendrite numbers were averaged from multiple neurons at every distance. The graphs in Figure 4M plotted average debris particle numbers divided by average dendrite numbers (left panel) or by average terminal dendrite numbers (right panel). The polynomial fits were generated by the Sholl Analysis plugin. For measuring GFP-Lact labeling, a dendrite/debris mask was generated by thresholding the tdTom channel using fixed threshold (100, 255) for every Z slice. This mask was used to extract signals from the Lact-GFP channel in each Z slice. The resultant image stack was then maximum-projected for measuring Lact-GFP intensity on selected dendritic branches within the dendrite/debris mask. For measuring Lact-GFP background levels, empty epidermal regions in the maximum projection of the original image stack were selected. We measured 2 regions on dendrites and one region in the background for each image. For kymographs, we used a custom macro based on the Straighten function to extract 4-pixel wide area centered at selected dendrites. The maximum intensity pixel in the 4-pixel area at each distance

was used to generate a single-pixel line for each time frame. The final kymographs were displayed using the Fire lookup table (LUT).

**Statistical Analysis**

R was used to conduct statistical analyses and generate graphs. (*$p < 0.05$, **$p < 0.01$, and ***$p < 0.001$). Statistical significance was set at $p < 0.05$. Data acquisition and quantification were performed non-blinded. Acquisition was performed in ImageJ (batch processing for debris coverage and level, manually by hand for GFP-Lact binding) and Microsoft Excel, statistical analyses were performed using R. We used the following R packages: car, stats, multcomp for statistical analysis and ggplot2 for generating graphs. Some graphs were made in Excel using its native plotting functions. For the statistical analysis we ran the following tests, ANOVA (followed by Tukey's HSD) when depended variable was normally distributed and there was approximately equal variance across groups. When dependent variable was not normally distributed and variance was not equal across groups, we used Kruskal-Wallis (followed by Dunn's test) to test the null hypothesis that assumes that the samples (groups) are from identical populations. To check for whether the data fit a normal distribution, we generated qqPlots where we plotted all of the estimated residuals which are differences between expected versus observed values. We used the Levene test to check for equal variance within groups. For comparison between two groups we used a pairwise t-test, p-values adjusted with the Bonferroni method. Fisher's exact test was used to compare experimental percentages to controls using GraphPad's online tool (https://www.graphpad.com/quickcalcs/contingency1.cfm).

*Replication*

For all larval and adult imaging experiments, at least 3 biological replications were performed for each genotype and/or condition.

**SUPPLEMENTAL REFERENCES**


Brand, A.H., and Perrimon, N. (1993). Targeted gene expression as a means of altering cell fates and generating dominant phenotypes. Development 118, 401-415.

Chu, J., Haynes, R.D., Corbel, S.Y., Li, P., Gonzalez-Gonzalez, E., Burg, J.S., Ataie, N.J., Lam, A.J., Cranfill, P.J., Baird, M.A., *et al.* (2014). Non-invasive intravital imaging of cellular differentiation with a bright red-excitable fluorescent protein. Nat Methods 11, 572-578.

Dobritsa, A.A., van der Goes van Naters, W., Warr, C.G., Steinbrecht, R.A., and Carlson, J.R. (2003). Integrating the molecular and cellular basis of odor coding in the Drosophila antenna. Neuron 37, 827-841.

Han, C., Jan, L.Y., and Jan, Y.N. (2011). Enhancer-driven membrane markers for analysis of nonautonomous mechanisms reveal neuron-glia interactions in Drosophila. Proc Natl Acad Sci U S A 108, 9673-9678.

Han, C., Song, Y., Xiao, H., Wang, D., Franc, N.C., Jan, L.Y., and Jan, Y.N. (2014). Epidermal cells are the primary phagocytes in the fragmentation and clearance of degenerating dendrites in Drosophila. Neuron 81, 544-560.

Han, C., Wang, D., Soba, P., Zhu, S., Lin, X., Jan, L.Y., and Jan, Y.N. (2012). Integrins regulate repulsion-mediated dendritic patterning of drosophila sensory neurons by restricting dendrites in a 2D space. Neuron 73, 64-78.

Lee, T., and Luo, L. (1999). Mosaic analysis with a repressible cell marker for studies of gene function in neuronal morphogenesis. Neuron 22, 451-461.

MacDonald, J.M., Beach, M.G., Porpiglia, E., Sheehan, A.E., Watts, R.J., and Freeman, M.R. (2006). The Drosophila cell corpse engulfment receptor Draper mediates glial clearance of severed axons. Neuron 50, 869-881.

Mapes, J., Chen, Y.Z., Kim, A., Mitani, S., Kang, B.H., and Xue, D. (2012). CED-1, CED-7, and TTR-52 regulate surface phosphatidylserine expression on apoptotic and phagocytic cells. Curr Biol 22, 1267-1275.

McGuire, S.E., Le, P.T., Osborn, A.J., Matsumoto, K., and Davis, R.L. (2003). Spatiotemporal rescue of memory dysfunction in Drosophila. Science 302, 1765-1768.

Pfeiffer, B.D., Truman, J.W., and Rubin, G.M. (2012). Using translational enhancers to increase transgene expression in Drosophila. Proc Natl Acad Sci U S A 109, 6626-6631.

Poe, A.R., Tang, L., Wang, B., Li, Y., Sapar, M.L., and Han, C. (2017). Dendritic space-filling requires a neuronal type-specific extracellular permissive signal in Drosophila. Proc Natl Acad Sci U S A 114, E8062-E8071.

Port, F., Chen, H.M., Lee, T., and Bullock, S.L. (2014). Optimized CRISPR/Cas tools for efficient germline and somatic genome engineering in Drosophila. Proc Natl Acad Sci U S A 111, E2967-2976.

Ren, X., Sun, J., Housden, B.E., Hu, Y., Roesel, C., Lin, S., Liu, L.P., Yang, Z., Mao, D., Sun, L., *et al.* (2013). Optimized gene editing technology for Drosophila melanogaster using germ line-specific Cas9. Proc Natl Acad Sci U S A 110, 19012-19017.

Suh, J.M., Gao, X., McKay, J., McKay, R., Salo, Z., and Graff, J.M. (2006). Hedgehog signaling plays a conserved role in inhibiting fat formation. Cell Metab 3, 25-34.